X-622-66-501

A QUASI-GLOBAL ANALYSIS OF TROPOSPHERIC WATER VAPOR CONTENT FROM TIROS IV RADIATION DATA

by

Ehrhard Raschke
Meteorologisches Institut
der Universität München, Germany

William R. Bandeen
Goddard Space Flight Center
Greenbelt, Maryland

1 September 1966

GODDARD SPACE FLIGHT CENTER
Greenbelt, Maryland

A QUASI-GLOBAL ANALYSIS OF TROPOSPHERIC WATER VAPOR CONTENT FROM TIROS IV RADIATION DATA

by
Ehrhard Raschke
Meteorologisches Institut
der Universität München, Germany

William R. Bandeen
Goddard Space Flight Center
Greenbelt, Maryland

ABSTRACT

Coordinated measurements of the earth's radiation to space within the 6.3μ band of water vapor and the 8 - 13μ atmospheric window were made over a five month period from February to June 1962 from the TIROS IV meteorological satellite. These measurements were analyzed to infer the spatial and temporal variations, on a quasi-global scale, of the following three quantities: (1) the mean relative humidity of the upper troposphere, (2) the mean effective temperature of the cloud top, land, or ocean surfaces, and (3) in conjunction with radiosonde temperature data, the water vapor mass above the 500 mb level.

The results show major regions of high moisture content over South America, Central Africa, and the western Pacific Ocean near the Intertropical Convergence Zone, plus several less prominent moist regions near the polar frontal zones in both hemispheres. The subtropical highs of both hemispheres are regions of low moisture content, as would be expected from the general circulation pattern in the troposphere.

At equatorial latitudes the average surface temperatures exhibit a persistent minimum along a narrow band identified with the Intertropical Convergence Zone. Elsewhere the magnitudes and patterns of the mean surface temperatures are

associated with semi-permanent regions, as well as with synoptic scale weather features along storm tracks in middle latitudes, especially during winter in each hemisphere.

The distribution pattern of water vapor mass above 500 mb strongly follows the 500 mb temperature field. Near the equator 0.3 - 0.4 gm cm^{-2} of precipatable water vapor are found, while in middle latitudes on the average only 0.02 - 0.04 gm cm^{-2} are present in the upper troposphere.

1. Introduction

In the past only a very few workers have investigated the global distributions of the total water vapor mass (e.g., Starr et al., 1958; Bannon and Steele, 1960), of the relative humidity of the troposphere (e.g., Száva-Kováts, 1938; Telegadas and London, 1954), and of precipitation (e.g., Möller, 1951; Geiger, 1964). These analyses were based largely on radiosonde measurements. However, the extreme sparsity of stations over most of the earth's surface and the sizable measurement errors cast doubt on the validity of these past analyses. Global satellite measurements of the thermal radiation from atmospheric water vapor over various parts of the electromagnetic spectrum promise to yield better determinations once methods are developed to extract from such measurements information about the vertical water vapor profile or the total water vapor content.

Such measurements have been made thus far, from the meteorological satellites TIROS II, TIROS III, and TIROS IV, only in one narrow spectral interval (5.7 - 6.9 microns) centered within the 6.3 micron band of water vapor; and most recently from the second generation meteorological satellite Nimbus II in an interval slightly displaced from that of TIROS. The outgoing radiance in the interval 5.7 - 6.9 microns is a measure of the mean relative humidity of the troposphere if the temperature distribution is assumed to be known (Möller, 1961). Since some radiation from boundary surfaces in the form of cloud tops also penetrates to space within this spectral interval, the temperature of these underlying surfaces must be known. Möller (1962) and later Raschke (1965) combined simultaneous measurements of the radiation between 5.7 and 6.9 microns and the radiation in the 8 - 13 micron atmospheric window to account for the temperatures

of high cloud surfaces. Their method, originally developed for evaluations of TIROS II and TIROS III measurements, is used here to evaluate the TIROS IV radiation data.

From the meteorological satellite TIROS IV, infrared and reflected solar radiation from the earth was measured in five different channels over a five-month period from February 8 to June 30, 1962 (Staff Members, 1963). An optical degradation of the sensors during this period necessitated correction of all the measured data (Staff Members, 1963; Bandeen et al., 1963). Some of the results are presented here, e.g., maps of monthly averages of (1) the mean relative humidity of the upper troposphere, (2) the effective surface temperature, and (3) the water vapor mass above 500 mb for February, April, and June 1962. Complete results and a comprehensive discussion of the research program are given in a Technical Report by Raschke (1966) to the NASA.

2. Principles of the Evaluation Method

The TIROS IV radiometer, having a relatively small field-of-view (about 5 degrees of arc) essentially measures the radiance in the direction of the satellite from the instantaneous spot viewed. The effective radiance $\bar{I}$ of upward-going infrared radiation within a spectral interval described by the instrumental response function ϕ_ν (filter function) can be calculated with the equation of radiative transfer for a concentrically stratified atmosphere in thermodynamic equilibrium and containing no scatterers:

$$\bar{I}(N) = \int_o^\infty \phi_\nu B_\nu\left[T(\log p_o)\right]\tau_\nu\left[N,\ w(\log p_o)\right]d\nu$$

$$+\int_o^\infty \int_{\log p_o}^{\log p_s} \phi_\nu B_\nu\left[T(\log p)\right] \frac{\partial\tau_\nu\left[N,\ w(\log p)\right]}{\partial \log p} d\log p\, d\nu, \quad (1)$$

where N is the nadir angle of measurement, ν the wave number, B_ν the Planck radiance at ν, T the ambient temperature, p the ambient pressure, and τ_ν the spectral transmittance of the atmosphere between a level at ambient pressure and the satellite if w is the absorbing gas mass in the vertical between both levels. If more gases than one participate in the radiative transfer in the spectral range described by the response function ϕ_ν, the function τ_ν, must be replaced by the product of the spectral transmittances for each gas. The subscripts "s" and "o" refer to the satellite and the lower boundary, respectively.

The total value of $\bar{I}(N)$ consists of contributions of radiation emitted from the lower boundary (first term) and from gases within the atmosphere above that boundary (second term). Between 5.7 and 6.9 microns the absorptivity of water vapor is so high that radiation emitted from the ground and from layers in the lower troposphere is absorbed completely in higher layers. Therefore, the 6.3 micron channel (Channel 1) of TIROS IV mainly receives radiation emitted from water vapor in the upper troposphere. According to Möller's (1961) findings, the 6.3 micron channel values are a measure of the mean relative humidity of the troposphere above about 600 mb in the absence of clouds.

Figure 1 shows that the 6.3 micron channel primarily measures thermal radiation from water vapor in layers between about 600 mb and 200 mb. Contributions below 600 mb are small because most of that radiation is absorbed before reaching space, while contributions from above 200 mb are small because of the very slight amount of water vapor. Figure 1 shows the weighted contributions of different layers in a tropical model atmosphere (cf. Figure 2) to the integrated outgoing radiance sensed by the 6.3 micron channel for mean tropospheric relative humidities of 5% and 100% at nadir angles of 0° and 40° (equivalent to zenith angles at the surface of 0° and 46° respectively for the TIROS IV mean orbital height of 778 km). It is seen that the moister atmosphere moves the weighting function upward into colder tropospheric temperatures, resulting in lower radiance measurements than for the corresponding drier atmosphere. An increase in the nadir angle also moves the weighting function upward.

From Figure 1 is is seen that, whereas in clear skies no radiation from the lower boundary is detected by the 6.3 micron channel and the first term in Equation (1) becomes zero, over high clouds radiation from the lower boundary (cloud tops) is detected by the 6.3 micron channel, and the first term as well as the second term in Equation (1) becomes important. To account for these clouds, Möller (1962) used simultaneous measurements of the upward radiation in the atmospheric window between 8 and 13 microns (detected by Channel 2 of the TIROS IV radiometer) to yield the temperature of the lower boundary.

The final evaluation procedure consists of comparing simultaneous measurements from the 6.3 micron and window channels with theoretically calculated measurements from model atmospheres. Calculations were carried out for the four model atmospheres (from Cole and Kantor, 1963) shown in Figure 2.

Evaluations of satellite data from a given latitude and season were carried out using whichever model atmosphere in Figure 2 most nearly corresponded to the climatological tabulations given by Kantor and Cole (1965). A constant relative humidity was assumed throughout the troposphere. A constant mixing ratio of water vapor to air of 2×10^{-6} gm/gm (after Masterbrook, 1963) was assumed at heights above 100 mb. A line of constant frost-point gradient connected the tropopause with the 100 mb level. For calculations of the upward radiation in the spectral range of the window channel, carbon dioxide (at a constant mixing ratio of 0.00031 parts by volume) and ozone (using profiles for different latitudes from Paetzold and Piscalar, 1961) were taken into account in addition to water vapor. Cloud surfaces and the ground were both assumed to radiate as black bodies at a temperature equal to that of the air directly above them.

All calculations were carried out with the computer program developed by Wark, Yamamoto, and Lienesch (1962). From the results thus obtained for different tropospheric relative humidities and for different cloud heights (and temperatures), evaluation diagrams were constructed. The diagram for radiation emerging vertically ($N = 0$) from the tropical model atmosphere is shown in Figure 3. In this diagram the pattern of isolines for different equivalent blackbody temperatures T_{bb} (corresponding to values of effective radiance detected by each channel) shows the influence of tropospheric water vapor on the radiative transfer in both spectral intervals. With increasing surface temperature the curves for the 6.3 micron channel turn markedly from the vertical to the horizontal, while those for the window channel change their direction only slightly.

The right hand side of the diagram represents soundings over clear areas or areas with low clouds. It is extended to surface temperatures higher than those given in the profiles in Figure 2, assuming that only the surface temperature increases while all other conditions remain constant. On this side the results are determined by the coördinates of points of intersection between two curves whose parameters are given by the satellite measurements. On the left hand side of the diagram the curves for the 6.3 micron channel measurements change their direction only slightly, indicating that over high, cold clouds the radiation detected by this channel comes primarily from the cloud surface. At equivalent blackbody temperature measurements by both channels of less than 228° K, it has been assumed that the upper troposphere is nearly saturated (relative humidity = 99%), a consequence of its being filled with clouds. This assumption in fact seems to be very arbitrary, because from measurements of the upward radiation it is not possible to distinguish between a high, cold, thin cirrus layer that is not completely opaque and a warmer, thicker, and opaque cumulus or alto stratus layer.

The results which are obtained by this method of interpretation are:

(1) values of a weighted average of the relative humidity above clouds (except above very high clouds), and

(2) an effective surface temperature of the underlying boundary.

Both of these quantities have been determined for ideal model stratifications only, viz., a mean climatological temperature profile and a cloudless and dustless upper troposphere bounded below by a black emitting surface. Errors arising from deviations of the actual atmospheric conditions from the model assumptions have been discussed extensively by Raschke (1965). They are

mainly caused by high, cold, but semi-transparent clouds and dust layers, which have other optical properties than the gases (Zdunkowski et al., 1965). Aerosols also affect the radiative transfer by absorption and emission (Robinson, 1962; Leupolt, 1965). The emissivity of the ground (e.g., Buettner and Kern, 1965; Hovis, 1966) and of cloud surfaces (Deirmendjian, 1960 and 1962; Havard, 1960) is less than unity and appears likely to be unequal in the two spectral intervals.

3. Evaluation Procedure

Data from both channels were affected by a degradation of the instrumental response while in orbit (Staff Members, 1963; Bandeen et al., 1963), and corrections for degradation were applied at the outset of the analysis. The correction nomogram for the Channel 2 (8 - 13 microns) data, taken from the TIROS IV Manual (Staff Members, 1963) is shown in Figure 4. Here the corrections are given in terms of an increment ($T_{bb} - T'_{bb}$) to be added to the measured equivalent black body temperature, T'_{bb}, to yield the correct value, T_{bb}. Parametric curves of T'_{bb} are shown, and the abscissa is scaled in terms of "Julian Days", i.e., the number of days after the launch of TIROS IV (launch day is Julian Day 0). (The term "Julian Day" as used here is a misnomer, and was changed to "TIROS Day" for subsequent TIROS satellites.) Since the degradation of Channel 2 was found to be symmetrical i.e., at a given time the degradation of data obtained through either the "floor" or the "wall" direction of view of the radiometer was the same (Staff Members, 1963) — only a single family of curves is shown in Figure 4.

The correction nomogram for the Channel 1 (5.7 - 6.9 microns) data as given in the TIROS IV Manual (Staff Members, 1963) also indicates symmetrical

degradation. However, a further study indicated that the degradation of Channel 1 data was asymmetrical instead, i.e., at a given time the degradation of data obtained through the floor direction of the radiometer generally differed from that of data obtained through the wall direction. These conclusions derived from a statistical study of the correlation of uncorrected Channel 1 measurements with corrected Channel 2 measurements (corrected by Figure 4). By assuming, that (1) the Channel 2 corrections were valid throughout the radiometer's lifetime, (2) the correlation in tropical latitudes of simultaneous, undegraded Channel 1 and Channel 2 measurements is time-invariant, and (3) above very high thick clouds both channels measure approximately the same (undegraded) equivalent blackbody temperature (Figure 3), it was possible to derive the new correction nomogram for Channel 1 data shown in Figure 5. The asymmetrical nature of the degradation pattern thus deduced is indicated by the two separate families of curves in Figure 5, one for "floor" data and another for "wall" data. It is interesting to note that before Julian Day 52 wall measurements were higher than floor measurements (of equivalent targets) whereas after Julian Day 52 the pattern reversed.

After instrumental degradation corrections were applied to individual measurements from both channels in the computer program, the data were categorized into three nadir angle intervals: 0°-26°, 26°-36°, and 36°-45°. All data corresponding to nadir angles greater than 45° were rejected because of interpretive problems associated with the increasingly important limb effects (Figure 1) and possible space contamination of measurements made near the horizon. For each of the nadir angle intervals, the data from each orbit were averaged over a square mesh grid, related to latitude and longitude on a Mercator map projection where

1 mesh interval = 5 degrees of longitude (Staff Members, 1962). Thus on a Mercator projection one grid element on the equator corresponded to 5 degrees of longitude × 5 degrees of latitude, whereas at latitude 60 degrees one grid element corresponded to 5 degrees of longitude × 2.5 degrees of latitude. The averaging of data from each orbit in this way was necessary to reduce the effects of a rather large random noise component in the channel 1 data (Staff Members, 1963), although in doing so, the simultaneity of individual measurement pairs was lost. However, the resultant pairs of averaged measurements from each orbit were considered to be representative of a simultaneous measurement pair over the mean state of clouds and moisture for each orbit within each grid element. Evaluation diagrams (Figure 3) were constructed for the four model atmospheres shown in Figure 2 and for the three nadir angle intervals listed above, and every pair of averaged measurements was evaluated with the applicable diagram to yield relative humidities and surface temperatures in every grid element covered by a single orbit. These "orbital values" for each grid element were subsequently averaged further to yield ten-day and monthly maps of the mean relative humidity and effective surface temperature.

4. Mean Relative Humidity of the Upper Troposphere and Effective Surface Temperature

Monthly averages of the mean upper tropospheric relative humidity and of the effective surface temperature are shown in Figures 6 - 11 for February, April, and June 1962. Isolines of relative humidity were drawn for 10, 20, 40, 60, and 80%; those of effective surface temperature were drawn for every 10 K. Stippling indicates areas where no measurements were acquired, largely because of orbital characteristics and ground station locations (Staff Members, 1963).

Generally the patterns of both quantities correspond to those which would be expected from a knowledge of the general circulation in the troposphere. Moist areas with relative humidities over 60% occur along the Intertropical Convergence Zone over the western Pacific (over Malaysia and Indonesia during February and over the monsoon areas of south and southeast Asia in June), over South and Central America, and over Central Africa. In these areas, known to be the areas of highest precipitation (e.g. see Möller, 1951; Geiger, 1964), upward motions of air cause upward water vapor transport and, hence, condensation. Therefore, the low temperatures of high cloud surfaces have mainly been measured; these then appear as cold "islands" in the surface temperature maps. High values of the relative humidities (and low surface temperatures) also are found along the polar frontal zones of both hemispheres, which are known to be areas of high cyclonic activity.

Subsidence of air in the upper and middle subtropical troposphere causes dry air and low cloudiness. Very dry areas over subtropical latitudes have been found with satellite-measured relative humidities of less than 10%. These low values agree very well with direct measurements made with frost-point hygrometer soundings over the Kwajalein Atoll in November 1963 (Masterbrook, 1965). Masterbrook found relative humidities there of less than 5% between 300 and 600 mb, which is the region of the upper troposphere from which the 5.7 - 6.9 micron channel primarily receives radiation (Figure 1).

Over the subtropical oceans the monthly averages of effective surface temperature are about 12 - 17 K lower than climatological values of the water surface temperature, indicating low trade wind clouds or a small mean cloudiness during the one month period. Remarkably high temperatures are found in February over

the Ethiopian Plateau and the Sudan. This is the dry season when the mean cloudiness over these regions is the lowest of the entire African Continent (Haurwitz and Austin, 1944). In later months, the highest values of the mean surface temperature occur mainly over the deserts of North Africa and Arabia where the minimum summer values of mean cloudiness are found (Haurwitz and Austin, 1944).

The migration northward of dry and moist belts and of warm and cold belts from February to June is clearly illustrated in the monthly maps and also in plots of ten-day zonal averages of both quantities versus time shown in Figures 12 and 13. In both of these figures the Intertropical Convergence Zone, identified by high relative humidities (40 - 60%) and low effective temperatures (< 270 K), moves with the season from the Southern to the Northern Hemisphere. Figure 12 shows that the subtropical regions of the winter hemispheres are very dry (~ 15% R.H.) as compared to the summer hemisphere. Also, in Figure 13 it is seen that the effective surface temperatures of the winter subtropics in the Northern Hemisphere are 5 - 8 K warmer than their counterparts of the Southern Hemisphere winter subtropics. This contrast probably arises from the different distributions of land and ocean over the two hemispheres.

The spatial coincidence of many moist and cold areas in the maps (excluding those very cold areas where the T_{bb} values of both channels were less than 228K and the relative humidity was set at 99%; cf. Section 2 above) leads to the suggestion that the relative humidity generally is high above clouds (Möller and Raschke, 1963). This relationship might also be due to an additional thin and partially transparent cirrus layer over most of the cloud fields, or to the fact that the emissivity of clouds in the 5.7 - 6.9 micron region is higher than in the

8 - 13 micron region (Havard, 1960). To investigate these possibilities the correlation coefficient R between relative humidities and surface temperatures was calculated for all orbits during the month of March 1962. When all of the data were correlated the result was R = -0.54. When data involving high, cold clouds were eliminated from the sample by accepting only measurements wherein the effective surface temperature exceeded 270 K, the result was R = -0.35. The considerably higher value of R over all data requires an even higher negative correlation between the low surface temperatures of high clouds and the inferred relative humidity of the air above. These statistics cast some doubt on the validity of the method above high cold clouds where the relative humidity of the air might be supposed to be as variable as it is above low clouds. It is pointed out that if one of the biasing mechanisms suggested above is operating, the resulting abnormally high relative humidities determined for the air above high cold clouds would tend to be compensated by the necessarily high relative humidities within the clouds themselves (although in theory the method does not consider the air within the cloud). Clearly, additional work is required on the interpretation of the data above high, cold clouds.

5. Water Vapor Mass Above 500 mb

The total water vapor mass above 500 mb was estimated by assuming that the values of the satellite determined mean relative humidity are representative of the atmosphere above 500 mb (Figure 1) and that the air temperature at the 500 mb level is known. The applicable temperature profile according to latitude and season from Figure 2 was selected and displaced slightly in the vertical as required to intersect the known 500 mb temperature. The moisture profile was constructed in accordance with Section 2 above. Thus for given values of the

mean relative humidity, the 500 mb temperature, and the latitude and season, the water vapor mass above 500 mb is uniquely determined.

The values of the mean upper tropospheric relative humidity were taken from Figures 6, 8, and 10. The 500 mb temperature fields were constructed from the "Monthly Climatic Data for the World" (USWB, 1962), and the latitude and season were known from the basic radiation data documentation. The resulting monthly maps of the total water vapor mass above 500 mb between 55° N and 55° S during February, April, and June 1962 are shown in Figures 14, 15 and 16. Isolines were drawn for 0.01, 0.02, 0.04, 0.06, 0.08, 0.1, 0.2, 0.3, and 0.4 gm cm^{-2} of precipitable water vapor. The patterns in all of these Figures show that, in general, high amounts occur in the tropics and low amounts occur at high latitudes, indicating the dominant influence of the air temperature on the water vapor content of the troposphere. The warm tropical centers of high relative humidity over Southeast Asia, South America, and Central Africa (cf. Figures 6, 8, and 10) are reflected in Figures 14, 15, and 16 as centers of the largest (> 0.3 gm cm^{-2}) amounts of water vapor. These areas are known to be areas of highest precipitation. By comparison, the comparatively cold high latitude regions, although having high relative humidities, have very low amounts of water vapor, emphasizing the strong dependence of water vapor mass on the air temperature. These distributions agree satisfactorily with those determined by Bannon and Steele (1960) from radiosonde measurements made during the years 1951-1955. A comparison of the three maps in Figures 14 - 16 shows the northward migration of the distinctive moisture patterns with the sun. These shifting patterns are brought out more clearly in Figure 17 where isolines of zonal averages of the water vapor mass are plotted against time after launch.

6. Conclusions

Coordinated infrared radiometric measurements in two spectral intervals from the TIROS IV meteorological satellite have been interpreted in terms of three parameters: (1) the mean upper tropospheric relative humidity, (2) the surface temperature of land, sea, or clouds, and (3) the water vapor mass above the 500 mb level. Strictly speaking such interpretations are possible only in a clear atmosphere above opaque, homogeneous clouds or other boundary surfaces which fill the instantaneous field-of-view of the radiometer and which radiate like black bodies in the two spectral intervals of interest. To the extent that these conditions are not met and to the extent that particulate matter (such as dust, ice crystals, and water droplets) enters into the transfer of radiation in the actual atmosphere, uncertainties are introduced into the results. Uncertainties also arise from the degradation of the radiometer calibration while the satellite is in orbit, but the effects of instrumental instability have largely been determined, and meaningful corrections can be applied to the measurements.

Despite these uncertainties, the results shown here over a period of nearly five months give a new insight into the role that water vapor may play in the climatology, general circulation, and heat budget of our planet. More accurate measurements of the water vapor content of the entire atmosphere should become possible from future meteorological satellites, such as the Nimbus series, in polar orbits and with improved instrumentation making measurements in several spectral intervals over a water vapor absorption band.

Acknowledgments

This research was sponsored by the National Aeronautics and Space Administration under Grant Ns G-305 to the University of Munich, Germany. The authors

wish to express their thanks to Professor Dr. Fritz Möller, Munich, for many valuable discussions during the course of these investigations. The formidable task of data processing was carried out by the staff of the Laboratory for Atmospheric and Biological Sciences, Goddard Space Flight Center. Special thanks are due to Mr. R. T. Hite and Mr. A. F. Simmons who carried out with meticulous care the very extensive computer programming without which this research could never have been accomplished.

References

Bandeen, W. R., R. E. Samuelson, and I. Strange, (1963): TIROS III Radiation Data Users' Manual Supplement. Goddard Space Flight Center, Greenbelt, Md., 56 pp.

Bannon, J. K., and L. P. Steele, (1960): Average Water Vapor Content of the Air. Geophys. Memoirs, No. 102, 13, London

Buettner, K. J. K., and C. D. Kern, (1965): Determination of Infrared Emissivities of Terrestrial Surfaces. Journ. Geoph. Res., 70, (6), 1329-1337

Cole, A. E. and A. J. Kantor, (1963): Air Force Interim Supplemental Atmospheres to 90 Kilometers. Air Force Surveys in Geophysics, No. 153. AFCRL-63-936 (available from NASA Scientific and Technical Information Facility, Document # N64-17320.)

Deirmendjian, D., 1960: Atmospheric extinction of infra-red radiation. Quart. J. R. Meteor. Soc., 86, 371-381

Deirmendjian, D., (1962): Scattering and Polarization Properties of Polydispersed Suspensions with Partial Absorption. RAND Memorandum RM-3228-PR, July 1962

Geiger, R., (1964): Die Atmosphäre der Erde. Julius Perthes, Darmstadt

Haurwitz, B. and J. M. Austin, 1944: Climatology. McGraw-Hill Book Company, Inc., New York, 410 pp.

Havard, J. B., (1960): On the Radiational Characteristics of Water Clouds at Infrared Wavelengths. Thesis at University of Washington. Defense Documentation Center, Document No. AD - 238 268

Hovis, W. A., Jr., 1966: Oplimum wavelength intervals for surface temperature radiometry. Applied Optics, 5 (5), 815-818

Kantor, A. J., and A. E. Cole, (1965): Monthly Atmospheric Structure, Surface to 80 km. Journ. Appl. Met., 4 (2), 228-237

Leupolt, A., (1965): Bestimmung der Kontinuumsabsorption im Spektralbereich von 0.5 bis 2.5 μm. Inauguraldissertation. Universität München, Meteorologisches Institut

Mastenbrook, H. J., (1963): Frost-Point Hygrometer Measurements in the Stratosphere and the Problem of Moisture Contamination. Humidity and Moisture, Vol. 2, Reinhold Public., 480-485.

Mastenbrook, H. J., (1965): The Vertical Distribution of Water Vapor over Kwajalein Atoll, Mashall Islands. U.S. Naval Research Laboratory Report 6367 (available from Defense Documentation Center (DDC), Document # AD 627 349.)

Möller, F., (1951): Vierteljahreskarten des Niederschlages für die ganze Erde. Petermanns Geographische Mitteilungen 95 (1). Quartalsheft, 1-7. Julius Perthes, Gotha

Möller, F., (1961): Atmospheric Water Vapor at 6-7 Microns from a Satellite. Planet. Space Sci., 5, 202-206

Möller, F., (1962): Einige vorläufige Auswertungen der Strahlungsmessungen von TIROS II. Arch. Met., Geophys. und Biokl., Serie B, 12, 78-93

Möller, F. und E. Raschke, (1963): Evaluation of TIROS III Radiation Data. Interim Report No. 1, Meteorologisches Institut der Universität München, NASA-Grant NsG-305 (also in NASA CR-112, 1964)

Paetzold, H. K. und P. Piscalar, (1961): Meridionale Ozonverteilung und stratosphärische Circulation. Naturwiss. 48, 474

Raschke, E., (1965): Auswertungen von infraroten Strahlungsmessungen des meteorologischen Satelliten TIROS III. Beitr. z. Phys. d. Atm., 38, 97-120, 153-187

Raschke, E., (1966): Tropospheric Water Vapor Content and Surface Temperatures from TIROS IV Radiation Data. Final Report, NASA Grant NsG-305, Meteorologisches Institut der Universität München. NASA CR-595, 1966

Robinson, E. D., (1962): Absorption of Solar Radiation by Atmospheric Aerosols, as Revealed by Measurements at the Ground. Arch. Met., Geophys. u. Biokl., Serie B, 12

Staff Members, Aeronomy and Meteorology Division, Goddard Space Flight Center and Meteorological Satellite Laboratory, USWB, 1962: TIROS III Radiation Data Catalog. Goddard Space Flight Center, Greenbelt, Md., 388 pp.

Staff Members, Aeronomy and Meteorology Division, Goddard Space Flight Center, 1963: TIROS IV Radiation Data Catalog and Users' Manual. Goddard Space Flight Center, Greenbelt, Md., 250 pp.

Starr, V. P., J. P. Peixoto, and G. C. Livadas, (1958): On the Meridional Flux of Water Vapor in the Northern Hemisphere. Geof. Pura e Appl., 39, 174-185

Száva-Kováts, J., (1938): Verteilung der Luftfeuchtigkeit auf der Erde. Ann. d. Hydr. u. Marit. Met., 60, 373-378

Telegadas, K., and J. London, (1954): A Physical Model of the Northern Hemisphere Troposphere for Winter and Summer. N. Y. Univ., Coll. of Eng., Sci-Rep. 1, AF 19 (122)-165

U.S.W.B., (1962): Monthly Climatic Data for the World (1962). U.S. Weather Bureau

Wark, D. Q., G. Yamamoto, and J. Lienesch, (1962): Methods of Estimating Infrared Flux and Surface Temperature from Meteorological Satellites. J. Atm. Sci., 19, 369-384

Zdunkowski, W., D. Henderson, J. V. Hales, (1965): The Influence of Haze on Infrared Radiation Measurements Detected by Space Vehicles. Tellus, 17, 147-165.

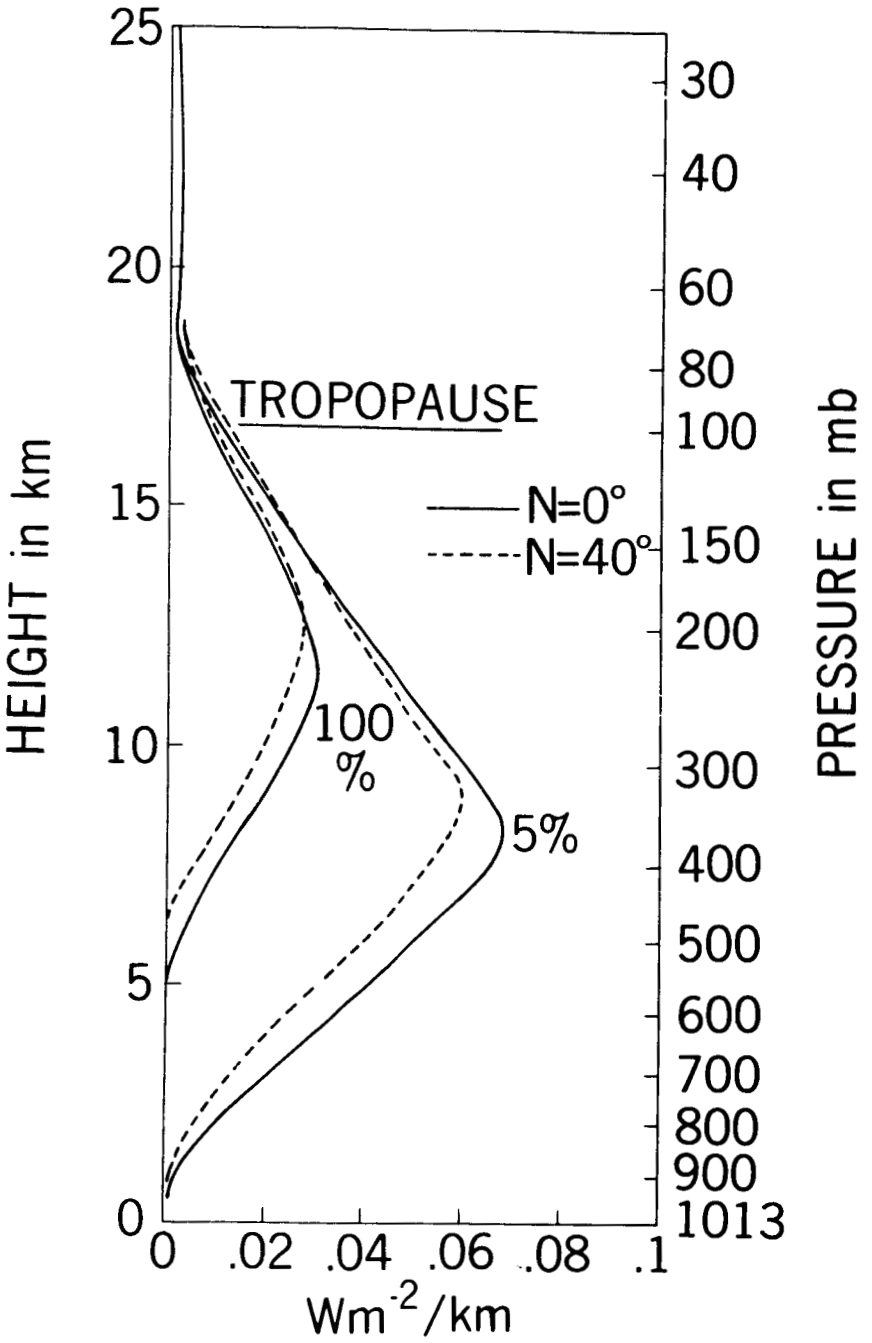

Figure 1—The contributions of layers of a cloudless tropical model atmosphere (Figure 2) to the outgoing effective radiance detected by the 5.7-6.9 micron channel of TIROS IV for two relative humidities (5%; 100%) and two nadir angles (N = 0°; 40°). The abscissa is shown in terms of $\pi\times$ the effective radiance per kilometer to conform to the radiometer calibration which isgiven in terms of effective radiant emittance (Staff Members, 1963).

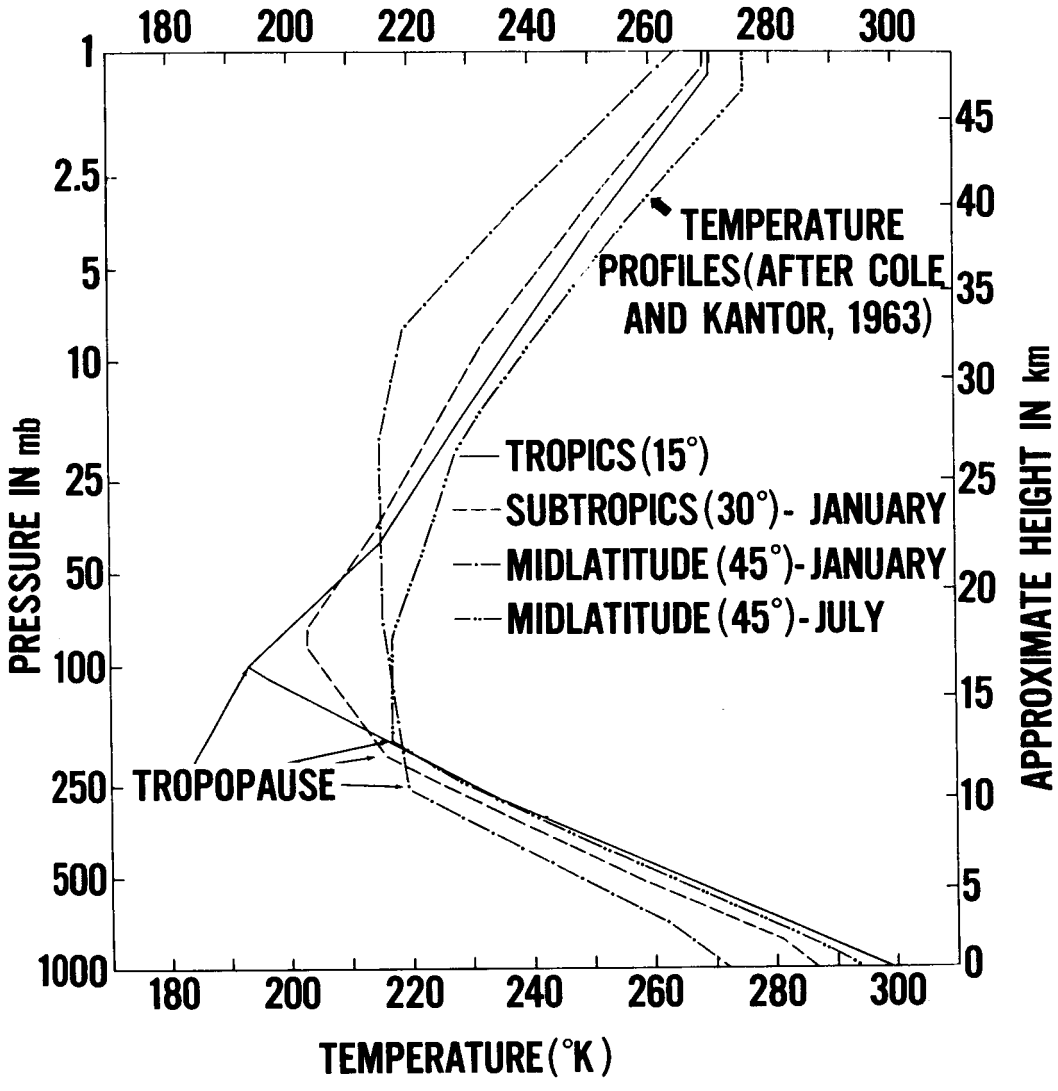

Figure 2-Model atmosphere temperature profiles.

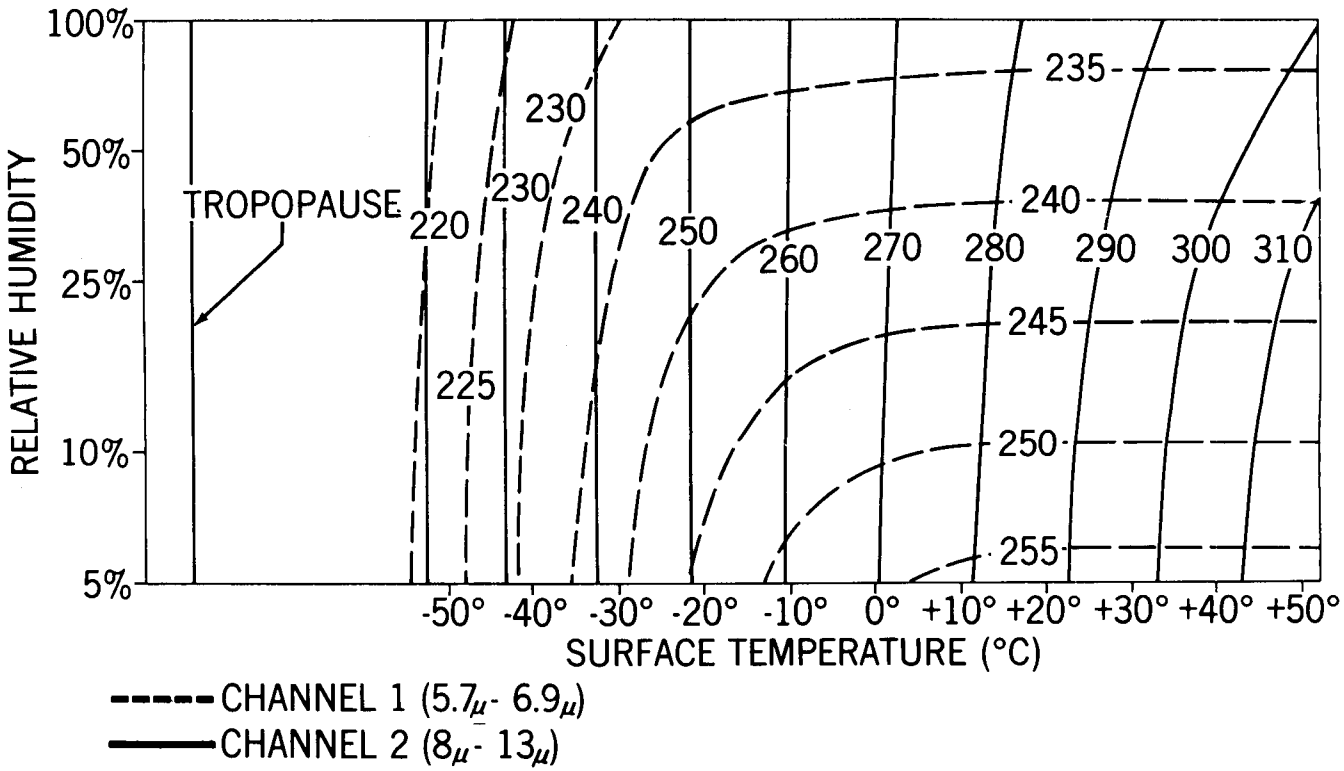

Figure 3-Evaluation diagram for vertically emerging radiation (N = O°) from the tropical model atmosphere.

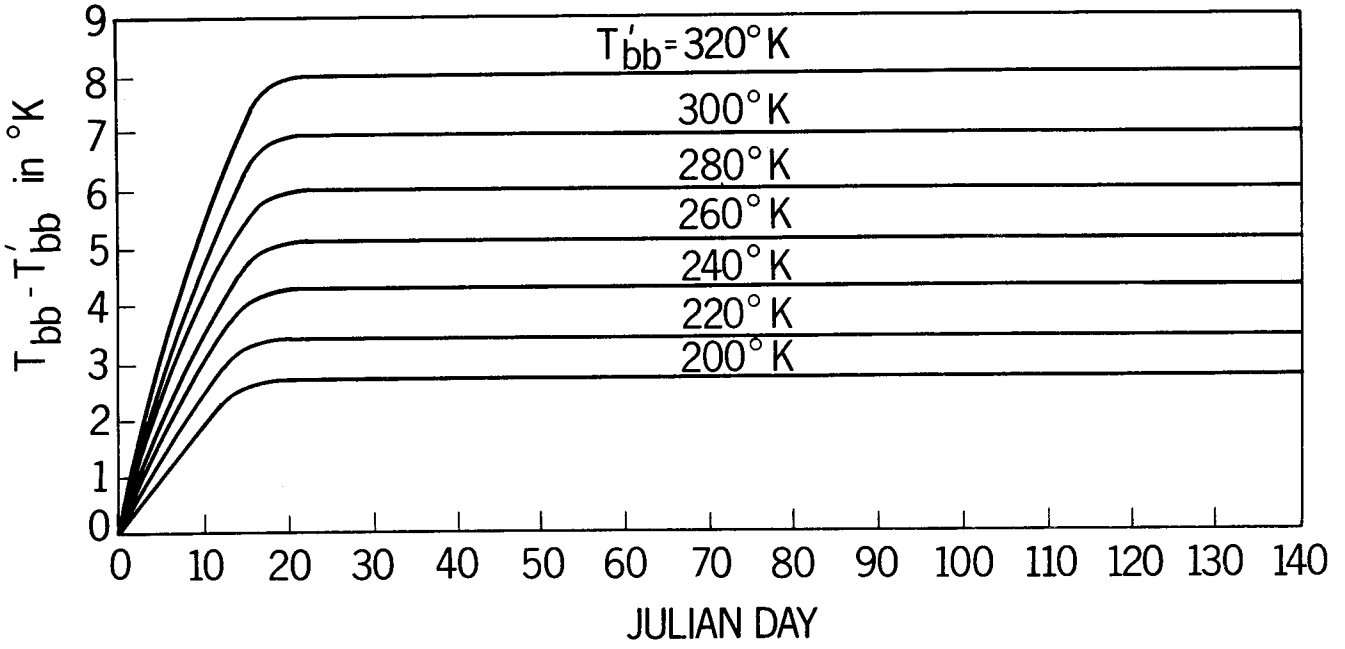

Figure 4—Symmetrical degradation corrections for both "floor" and "wall" directions of the 8-13 micron channel of TIROS IV vs. days after launch.

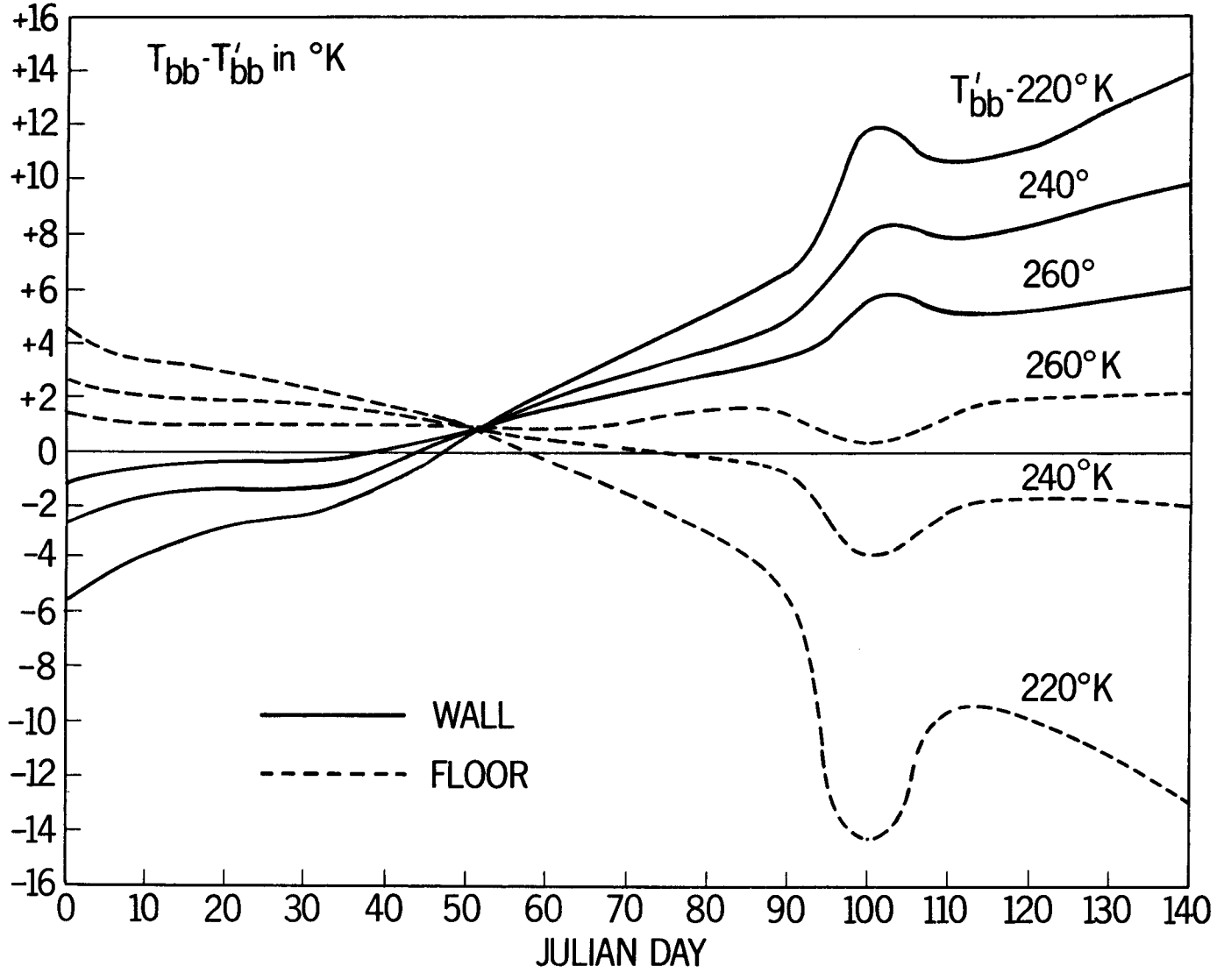

Figure 5—Asymmetrical degradation corrections for the "floor" and "wall" directions separately of the 5.7-6.9 micron channel of TIROS IV vs. days after launch.

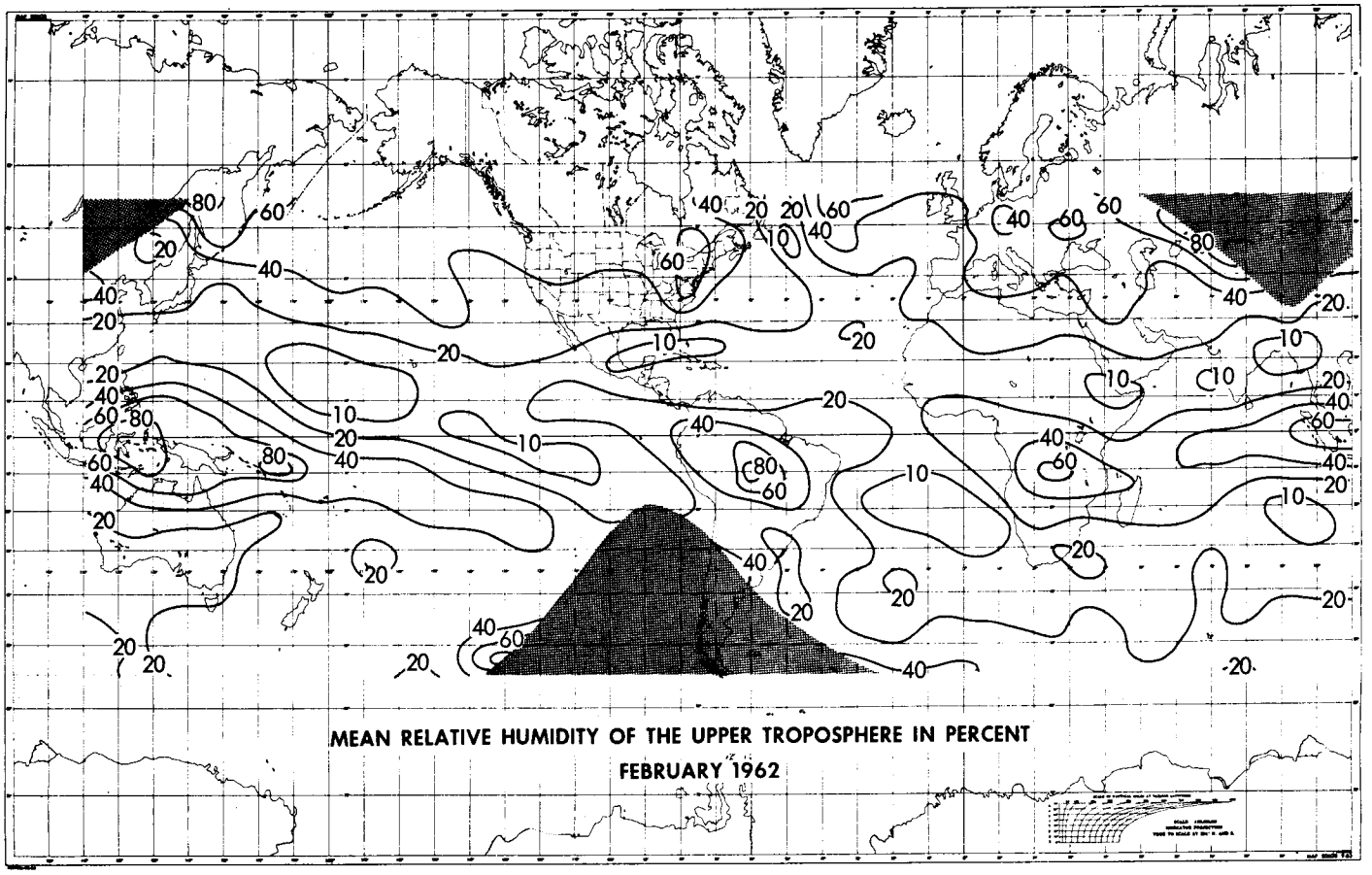

Figure 6—Quasi-global distribution of the mean relative humidity of the upper troposphere during February 1962 inferred from coördinated TIROS IV Channel 1 and Channel 2 radiometric measurements.

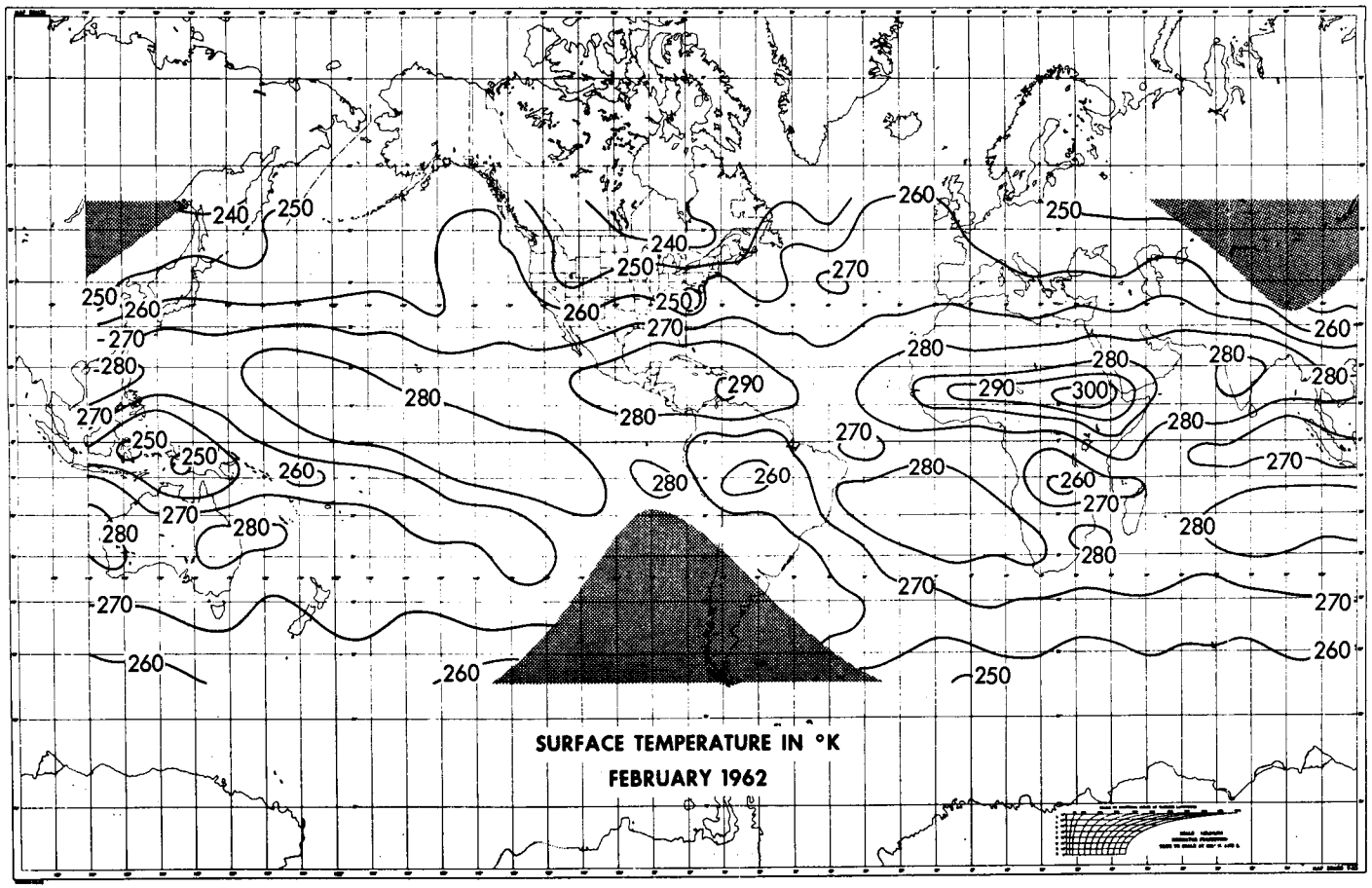

Figure 7—Quasi-global distribution of the effective surface temperature during February 1962 inferred from coördinated TIROS IV Channel 1 and Channel 2 radiometric measurements.

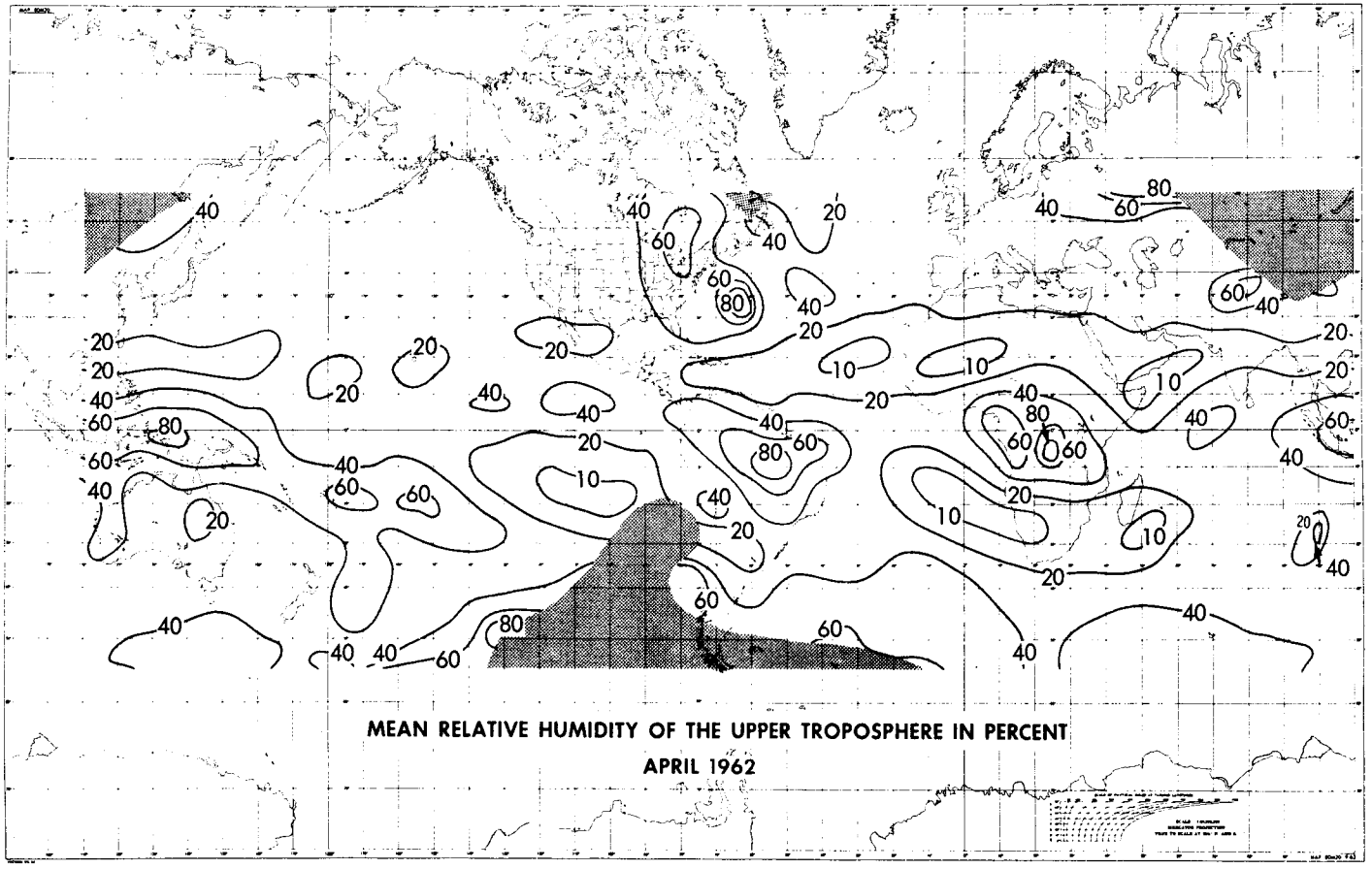

Figure 8—Quasi-global distribution of the mean relative humidity of the upper troposphere during April 1962 inferred from coördinated TIROS IV Channel 1 and Channel 2 radiometric measurements.

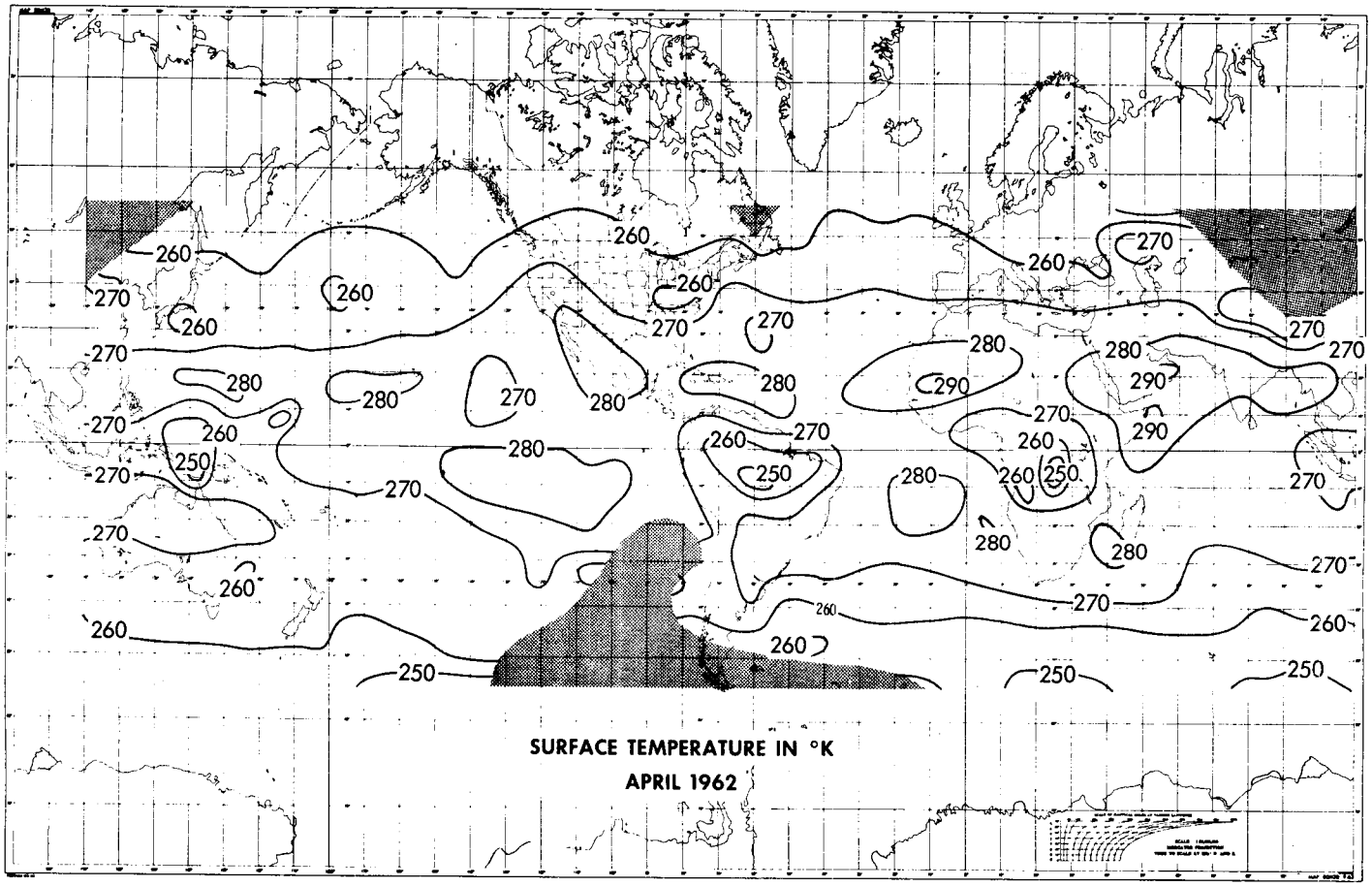

Figure 9—Quasi-global distribution of the effective surface temperature during April 1962 inferred from coördinated TIROS IV Channel 1 and Channel 2 radiometric measurements.

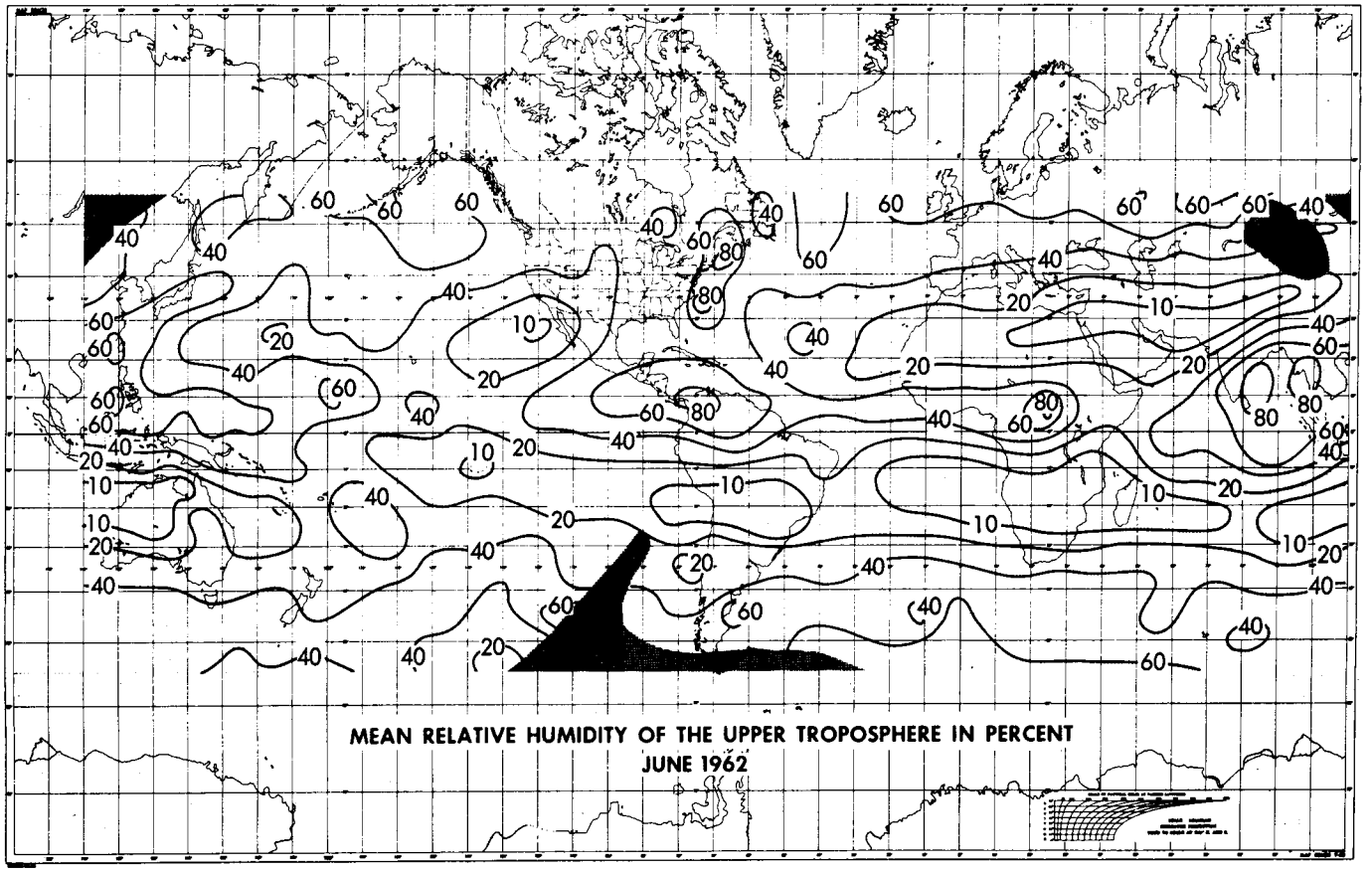

Figure 10—Quasi-global distribution of the mean relative humidity of the upper troposphere during June 1962 inferred from coördinated TIROS IV Channel 1 and Channel 2 radiometric measurements.

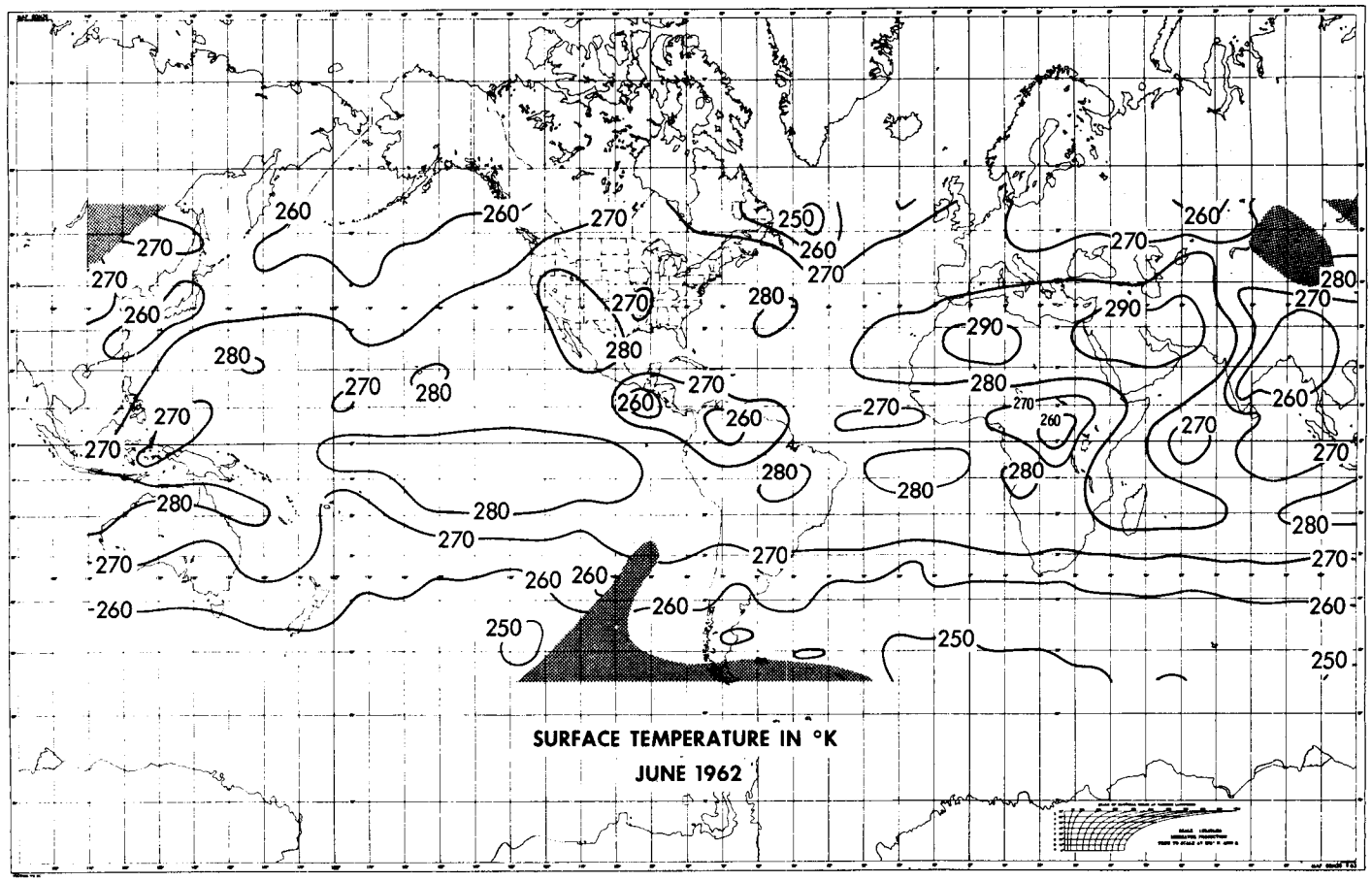

Figure 11—Quasi-global distribution of the effective surface temperature during June 1962 inferred from coördinated TIROS IV Channel 1 and Channel 2 radiometric measurements.

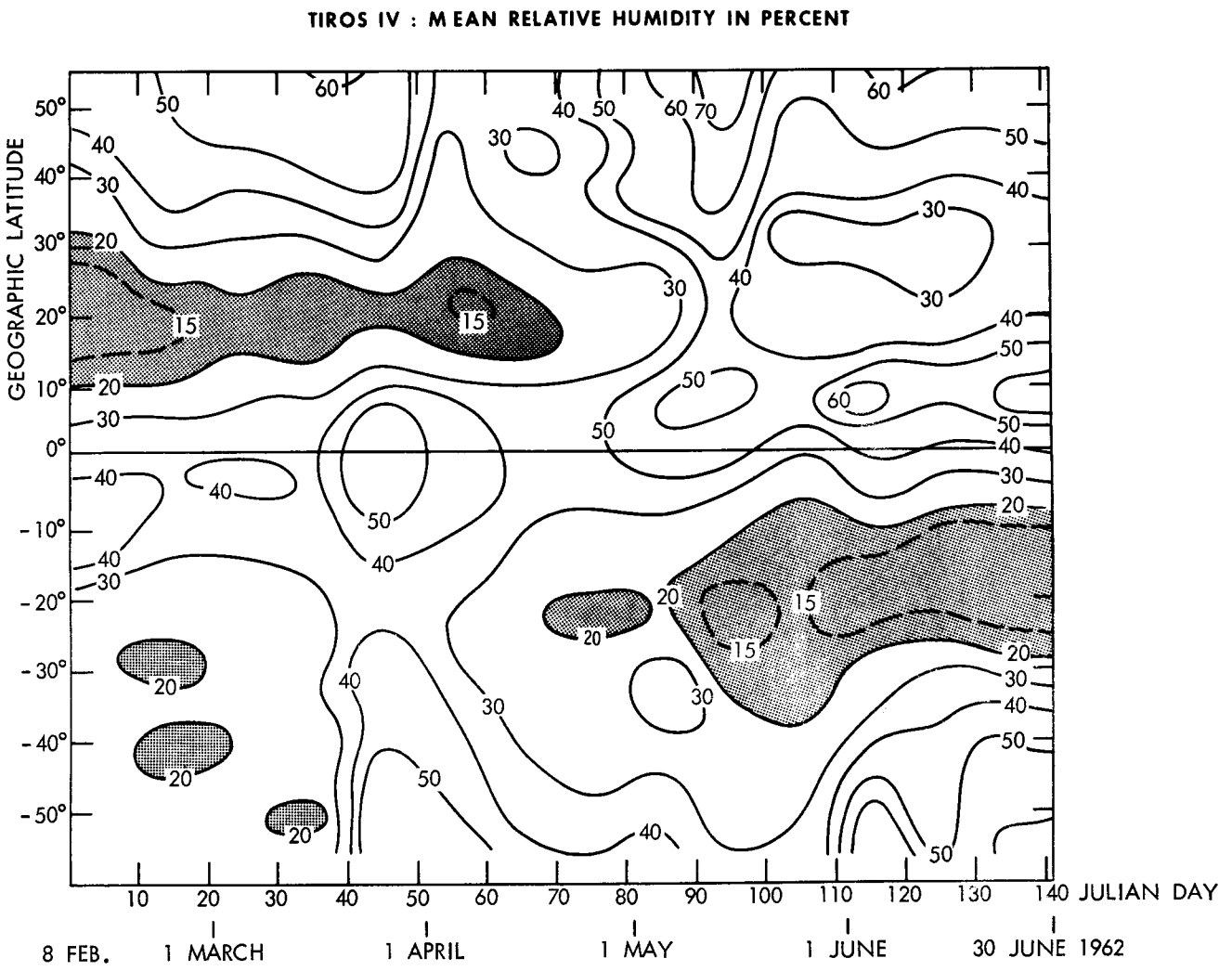

Figure 12—Zonal averages of the mean relative humidity of the upper troposphere inferred from coördinated TIROS IV radiometric measurements. These averages were determined for ten-day periods within zones of approximately 5 degrees of latitude.

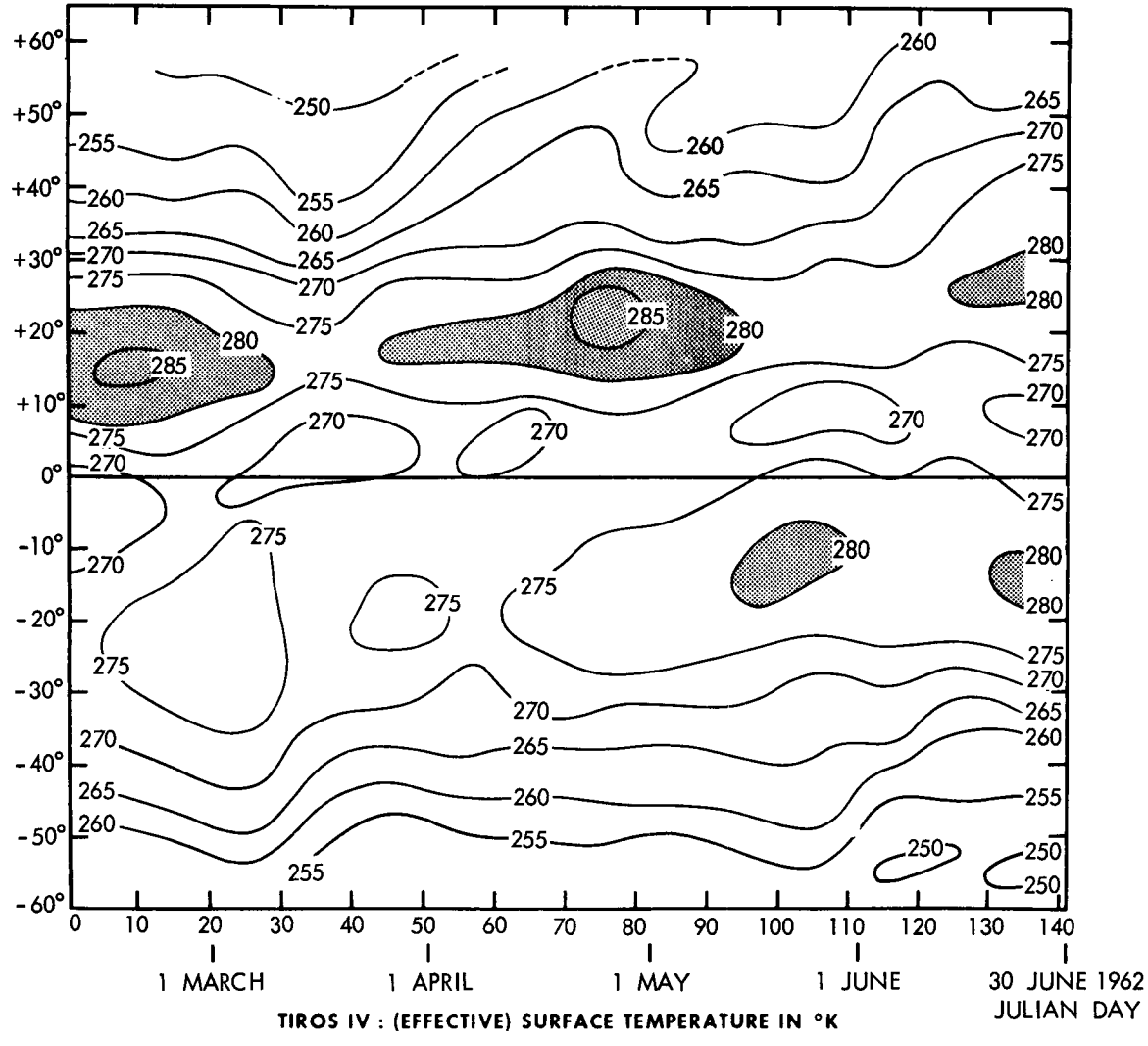

Figure 13—Zonal averages of the effective surface temperature inferred from coördinated TIROS IV radiometric measurements. These averages were determined for ten-day periods within zones of approximately 5 degrees of latitude.

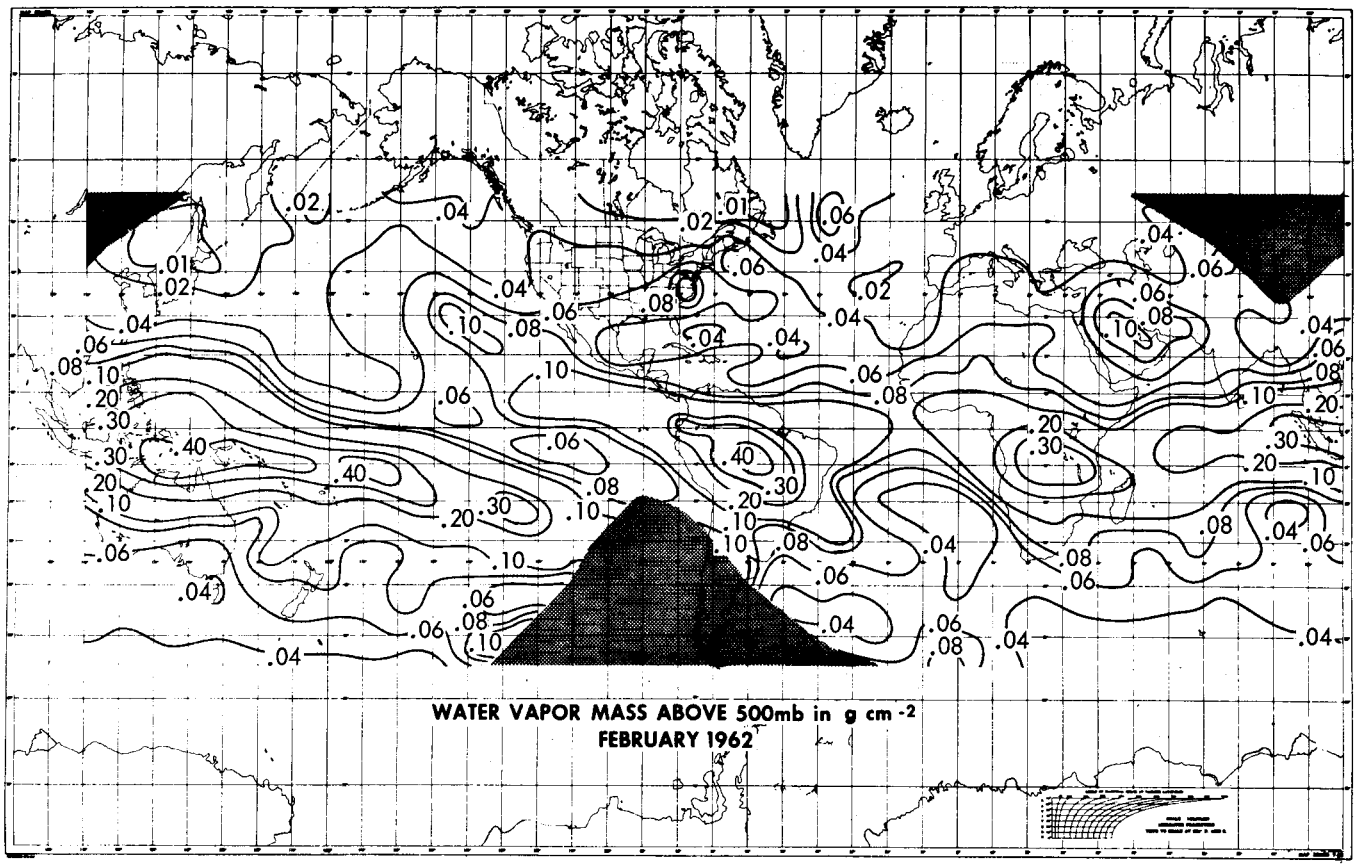

Figure 14—Quasi-global distribution of the water vapor mass above 500 mb during February 1962 inferred from coördinated TIROS IV Channel 1 and Channel 2 radiometric measurements.

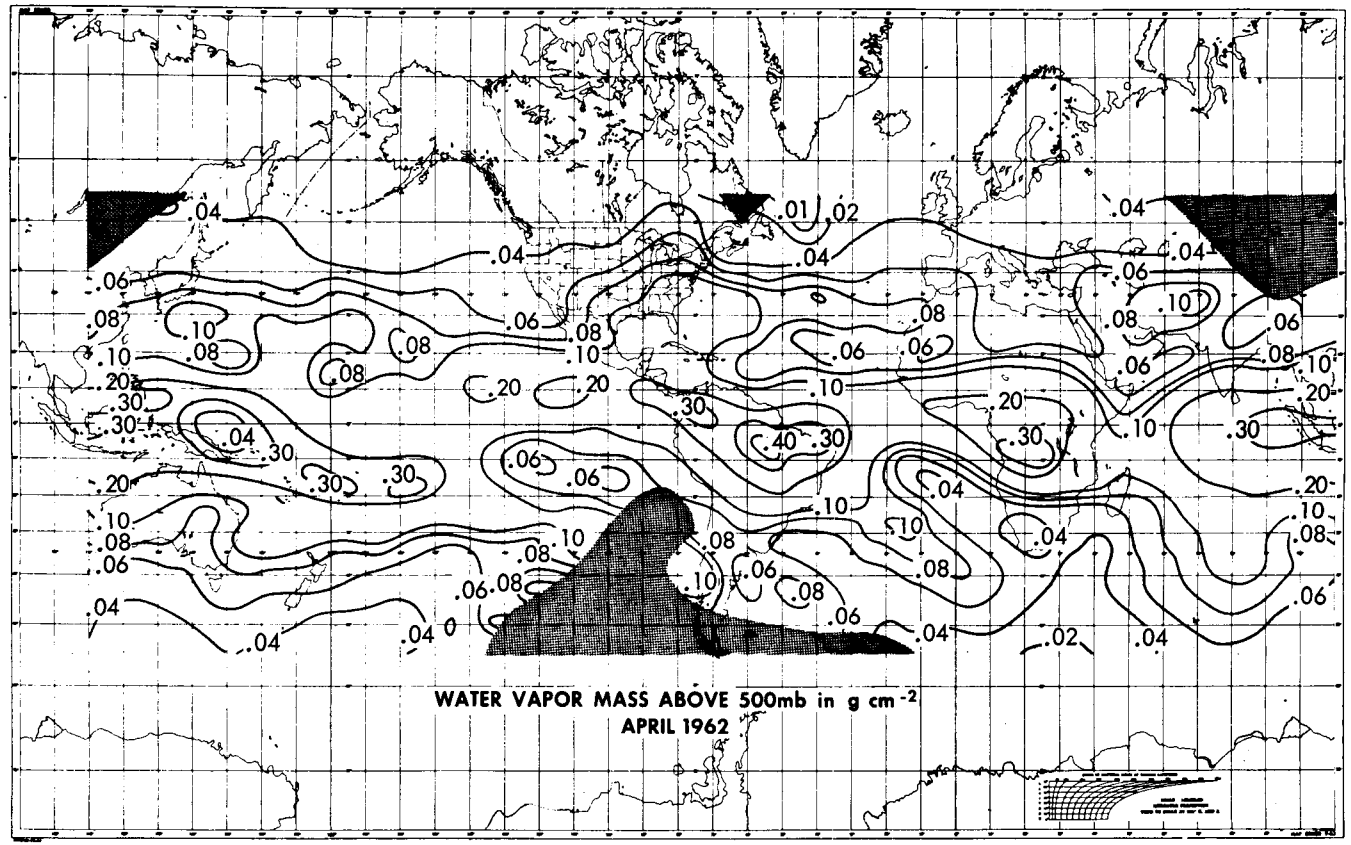

Figure 15—Quasi-global distribution of the water vapor mass above 500 mb during April 1962 inferred from coördinated TIROS IV Channel 1 and Channel 2 radiometric measurements.

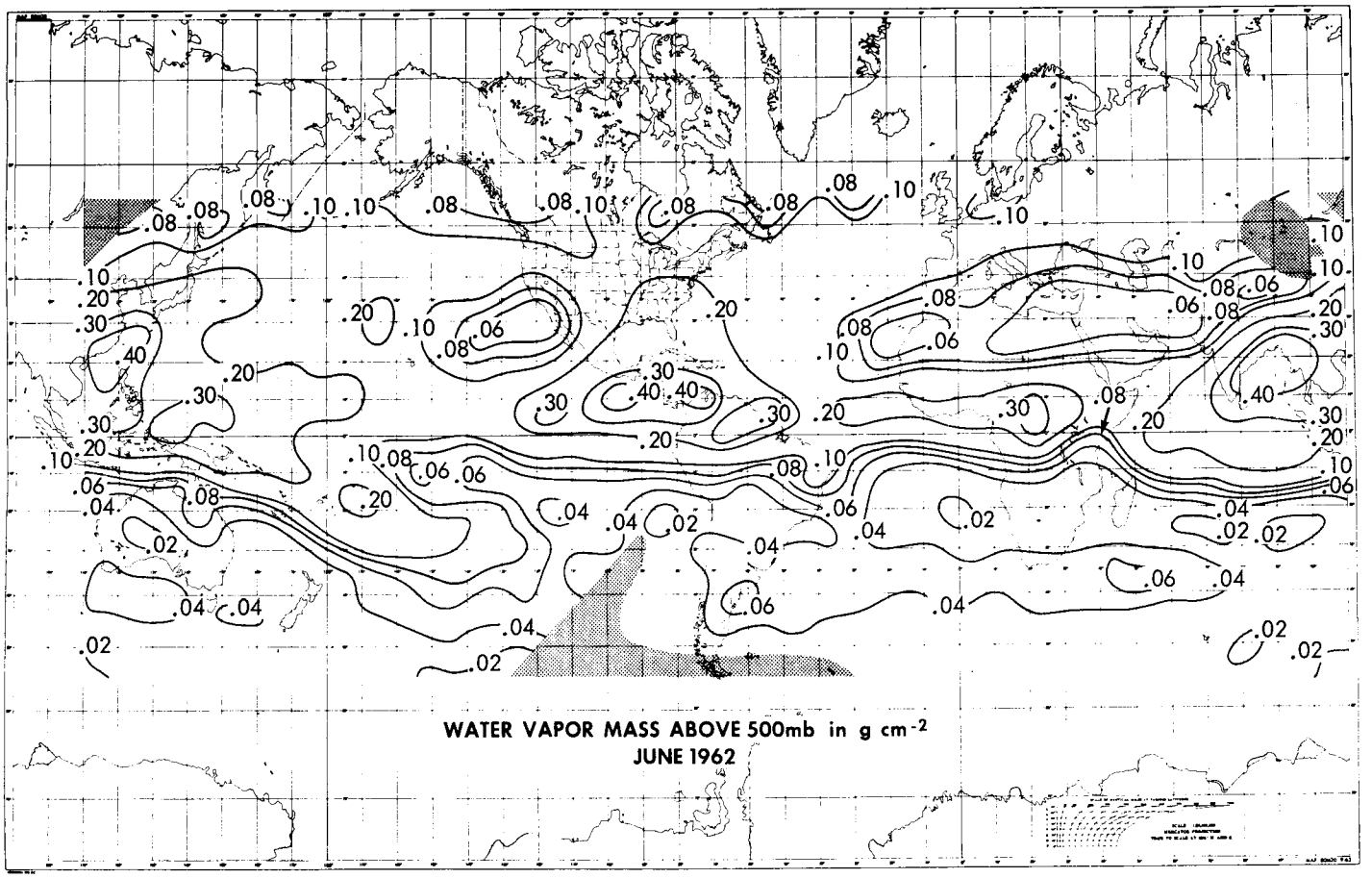

Figure 16—Quasi-global distribution of the water vapor mass above 500 mb during June 1962 inferred from coördinated TIROS IV Channel 1 and Channel 2 radiometric measurement.

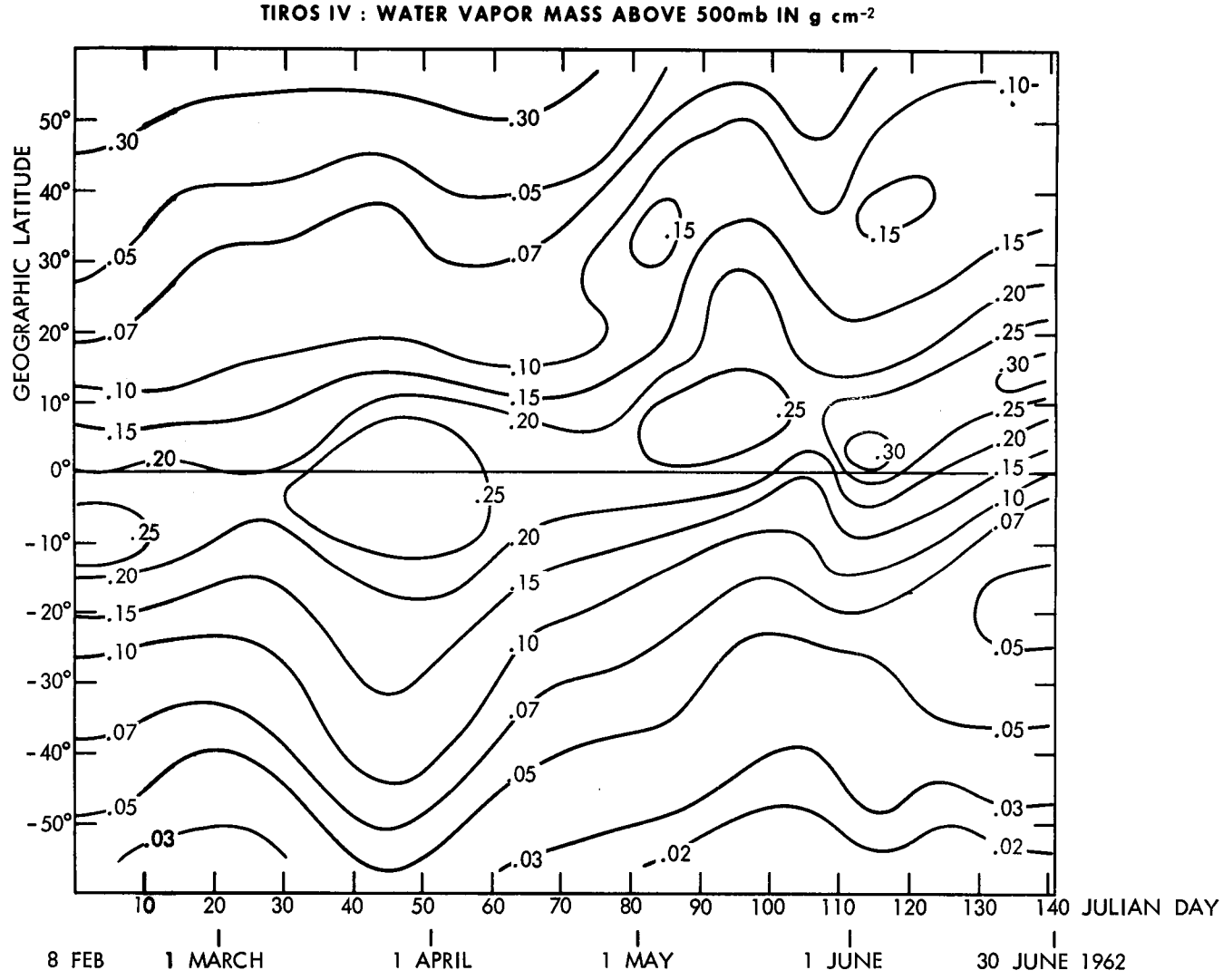

Figure 17—Zonal averages of the water vapor mass above 500 mb inferred from coordinated TIROS IV radiometric measurements. These averages were determined for ten-day periods within zones of approximately 5 degrees of latitude.